9. ANTHROPOGENIC AND NATURAL INFLUENCES ON RECORD 2016 MARINE HEAT WAVES

Eric C. J. Oliver, Sarah E. Perkins-Kirkpatrick, Neil J. Holbrook, and Nathaniel L. Bindoff

Two of the longest and most intense marine heat waves in 2016 were up to fifty times more likely due to anthropogenic climate change.

Introduction. In 2016 a quarter of the ocean surface experienced either the longest or most intense marine heatwave (Hobday et al. 2016) since satellite records began in 1982. Here we investigate two regions—Northern Australia (NA) and the Bering Sea/Gulf of Alaska (BSGA)—which, in 2016, experienced their most intense marine heat waves (MHWs) in the 35-year record. The NA event triggered mass bleaching of corals in the Great Barrier Reef (Hughes et al. 2017) while the BSGA event likely fed back on the atmosphere leading to modified rainfall and temperature patterns over North America, and it is feared it may lead to widespread species range shifts as was observed during the "Blob" marine heat wave which occurred immediately to the south over 2013–15 (Belles 2016; Cavole et al. 2016). Moreover, from a climate perspective it is interesting to take examples from climate zones with very different oceanographic characteristics (high-latitude and tropics). We demonstrate that these events were several times more likely due to human influences on the climate.

AFFILIATIONS: Oliver—Institute for Marine and Antarctic Studies, University of Tasmania, Hobart, and Australian Research Council Centre of Excellence for Climate System Science, Hobart, Australia, and Department of Oceanography, Dalhousie University, Halifax, Nova Scotia, Canada; Perkins-Kirkpatrick—Climate Change Research Centre, The University of New South Wales, Sydney, and Australian Research Council Centre of Excellence for Climate System Science, Sydney, Australia; Holbrook—Institute for Marine and Antarctic Studies, University of Tasmania, Hobart, and Australian Research Council Centre of Excellence for Climate System Science, Hobart, Australia; Bindoff—Institute for Marine and Antarctic Studies, University of Tasmania, Hobart, and Antarctic & Climate Ecosystem Cooperative Research Centre, University of Tasmania, Hobart, Australia

Data and methods. Observations consisted of sea surface temperatures (SSTs) from the daily NOAA OI SST v2 0.25° gridded dataset over 1982–2016 (Reynolds et al. 2007). We also used the in situ-based monthly HadISST 1° gridded dataset over 1900–2016 (Kennedy et al. 2011a,b). SST time series were generated by spatially averaging over (20°–5°S, 110°–155°E) for NA and (50°–65°N, 178°–127°W,) for the BSGA (Figs. 9.1a,b, black boxes). Anomalies were calculated relative to a base period of 1961–90. Daily climatologies were calculated from NOAA OI SST over the period 1982–2005, and in order to reference this to the chosen base period, we offset by the mean warming from 1961–90 to 1982–2005 calculated from HadISST (+0.19°C for both NA and BSGA; see Oliver et al. 2017 for more details).

Marine heat waves were defined as periods when SSTs were above the seasonally varying 90th percentile for at least five consecutive days (Oliver 2015; Hobday et al. 2016). We considered two MHW metrics: duration (time between the start and end dates) and maximum intensity (peak temperature anomaly).

We employed Coupled Model Intercomparison Project Phase 5 (CMIP5; Taylor et al. 2012) global climate model simulations of historical and projected future climates. We used daily SST outputs from the historicalNat (representing historical conditions without anthropogenic influence; models are forced by natural volcanic and solar forcing only) and the historical and RCP8.5 experiments (representing historical conditions with anthropogenic influence; models include anthropogenic greenhouse gas and aerosol forcing in addition to natural forcing) from seven models (Table ES9.1). Model climatologies were calculated using a base period of 1961–90; RCP8.5 anomalies were defined relative to the historical run climatology. The nonseasonal daily SST variance (i.e., after removing the climatology) was bias-corrected for each model based on the ratio between the standard deviations of the daily observations and the daily historical runs (see Oliver et al. 2017 for more details).
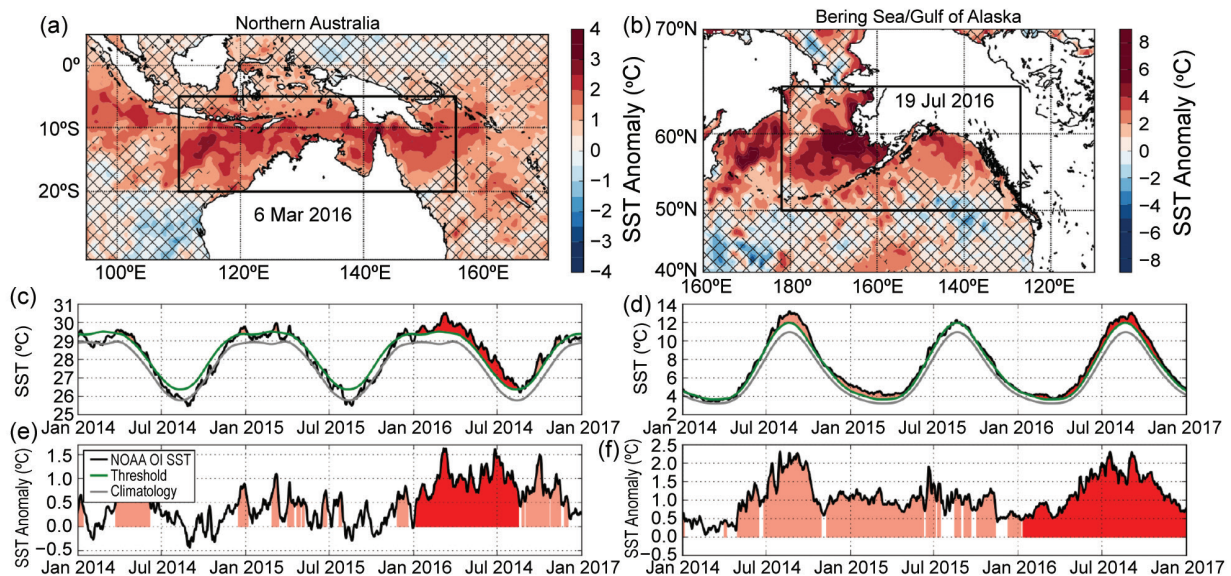
Fig. 9.1. 2016 MHWs in (left) NA and (right) BSGA. (a),(b) SST anomalies (°C) during the peak of each event (date indicated in panel) and unhatched areas indicate regions defined as MHW on that date according to the Hobday et al. (2016) definition. (c),(d) Daily SSTs (°C): NOAA OI SST (black), threshold (green), and 1961–90 climatology (gray) (e),(f) SST anomalies (°C) averaged over NA and BSGA during 2014–16. In (c)–(f) red shading indicates the 2016 MHW; lighter shading indicates other detected marine heat waves over the period.

MHWs were then identified in all model experiments using the Hobday et al. (2016) definition.

The fraction of attributable risk (FAR) methodology (Lewis and Karoly 2013; King et al. 2015) was used to examine how anthropogenic forcing modified likelihoods of the MHW events. Probability distributions (PDFs) of MHW durations and intensities were calculated from historicalNat (1850–2005, representative of the natural world) and RCP8.5 (2006–20, representative of the present day) experiments. We attributed event duration and intensity separately, and the value attributed was of the next least intense and next shortest event in the observed distribution (Lewis and Karoly 2013). The area of the PDF for values larger than that of the events being attributed was calculated to define the FAR statistic. We calculated 10 000 FAR values by bootstrap sampling with replacement (N = 14 random ensemble members sampled each iteration, half the total number of historical ensemble members), and quoted the first percentile of the resulting FAR distribution (with each ensemble weighted by the inverse of the number of ensembles for that particular model, thereby weighting equally across models). This quantified the degree to which we could be *virtually certain* (at least 99% probability in IPCC Fifth Assessment Report terminology; http://ipcc.ch/report/ar5/) that anthropogenic forcing modified the event likelihood. Return periods were estimated by taking the number of event occurrences

in a model experiment, dividing the total number of model years in that experiment (across all models and ensembles,) and then inverting. Note that the results presented here (FAR and return periods) are dependent on the models used and may change as the models are refined or if a different subset of models and experiments are used.

We also quantified the role of the dominant internally varying climate modes—noting that these two MHW events co-occurred with the 2015/16 El Niño, the negative phase of the Indian Ocean dipole (IOD) in 2016, and a strongly positive interdecadal Pacific oscillation (IPO) since 2014. Specifically, we examined how the probabilities of all MHWs in the records changed according to the phases of these three modes and quantified statistically how these modes modulated the likelihoods of MHWs generally, rather than the specific events considered above. Climate modes were quantified by the relevant indices calculated from the historicalNat experiment: the Niño-3.4 index, the dipole mode index (DMI), and the tripole mode index (TPI; see online supplement for details). All MHWs in the historicalNat simulations were identified and assigned the climate mode phases during the date of maximum MHW intensity. We compared the distributions of MHW intensities/durations according to their climate mode phases, using a Kolmogorov–Smirnov (KS) test to determine if the distributions were significantly different. We also cal-

culated whether the probability of occurrence of the MHWs were significantly modified according to the phases of the modes, and performed bootstrap resampling as above to estimate statistical significance.

Results. The 2016 marine heat waves in NA and BSGA were contiguous over broad swaths of the ocean (within the boxed regions: 4.76 Mkm² for NA, 2.45 Mkm² for BSGA; Figs. 9.1a,b). After averaging SSTs regionally, the NA event (Figs. 9.1c,e, red shading) was the most intense (maximum intensity of +1.6°C on 6 March 2016) and the second longest (224 days, 6 January–16 August 2016) on record; the BSGA event (Figs. 9.1d,f, red shading) was the most intense (maximum intensity of +2.3°C on 19 July 2016) and longest (≥355 days, 12 January 2016–31 December 2016, and extending into 2017 beyond the analysis period).

The probability distributions of NA and BSGA event intensities and durations from the observations and model runs, and the corresponding FAR values are shown in Fig. 9.2. For both intensity and duration, there were clear shifts towards larger events becoming more probable (Figs. 9.2a,b,e,f) in the 2006–20 world (RCP8.5, red lines) over the natural world (1850–2005, historicalNat, blue lines). The NA event intensity was *virtually certain* to be at least 8.5 times as likely in 2006–20 as compared to a natural world (Fig. 9.2c, dashed line) and NA event duration was *virtually certain* to be at least 53 times as likely in 2006–20 under anthropogenic climate change as compared to a natural world (Fig. 9.2g, dashed line). The BSGA event intensity was *virtually certain* to be at least 7.3 times as likely in 2006–20 as compared to a natural world (Fig. 9.2d, dashed line) and BSGA event duration was *virtually certain* to be at least 7.4 times as likely in 2006–20 under anthropogenic climate change as compared to a natural world (Fig. 9.2h, dashed line). Return periods of these events in the natural world were 1-in-970 years (NA duration), 1-in-170 years (NA intensity), 1-in-130 years (BSGA duration) and 1-in-120 years (BSGA intensity) and in all cases reduced to 1-in-5 years under anthropogenic forcing (RCP8.5, 2006–20).

The pattern of warming associated with anthropogenic forcing is more spatially uniform than the pattern of SST anomalies present during these events (Fig. ES9.1). Therefore, natural internal variability may have also played a role in the occurrence of these events (Table ES9.2). For NA, the distributions of MHW intensities and durations were significantly different between the DMI+ and DMI– phases ($p < 0.01$). The larger events, measured by the 90th percentiles of these distributions, showed MHWs as being longer in duration (74 vs. 40 days) but slightly less intense (0.99°C vs. 1.04°C) during DMI– phases. Frequency also showed a strong response: MHW events were significantly ($p < 0.01$) more/less frequent during DMI– (46.0%) / DMI+ (15.4%). There were no significant differences ($p > 0.01$) between the phases of Niño-3.4 or TPI for either MHW duration or intensity in the NA region; the frequency response was not significant for Niño-3.4 or TPI.

For the BSGA region, the distributions of MHW intensities were significantly different between DMI+ and DMI– phases ($p < 0.01$), with the 90th percentiles showing MHW events as being slightly more intense (1.39°C vs. 1.32°C) during the DMI+ phase. The distributions of durations were significantly different between Niño-3.4+ and Niño-3.4– phases ($p < 0.01$), with 90th percentiles showing MHW events being longer in duration (86 vs. 59 days) during the Niño-3.4+/- phase. The distributions of durations were also significantly different between TPI+ and TPI– phases ($p < 0.01$), with 90th percentiles showing MHW events being longer (85 vs. 65 days) during TPI+. Frequency also showed a significant ($p < 0.01$) response: 41.8% (39.3%) of MHW events occurred during Niño-3.4+ (TPI+) and only 19.3% (23.3%) during Niño-3.4– (TPI–); the frequency response was weaker (but significant) for DMI.

Conclusions. In 2016, both the NA and BSGA regions experienced their most intense MHWs across the 35-year satellite SST record. For BSGA, it was also the longest. We are *virtually certain* anthropogenic climate change played a role in increasing the likelihood of their event durations and intensities. Importantly, we find that there is attributable human influence regardless of the phase of El Niño, IOD, or IPO, although our findings suggest that natural internal variability also contributed to raising likelihoods. Specifically, we expect the negative IOD in 2016 to have played a role in increasing the NA region MHW event likelihood and duration and, interestingly, not the 2015/16 El Niño. We expect that the 2015/16 El Niño and positive IPO contributed to increasing the BSGA MHW event likelihood and duration in 2016. While both anthropogenic climate change and natural internal variability contributed to the occurrence of these extreme MHWs in 2016, the fact that anthropogenic forcing reduced return periods by a factor of up to two hundred indicated that it was extremely unlikely that natural variability alone led to the observed anomalies.
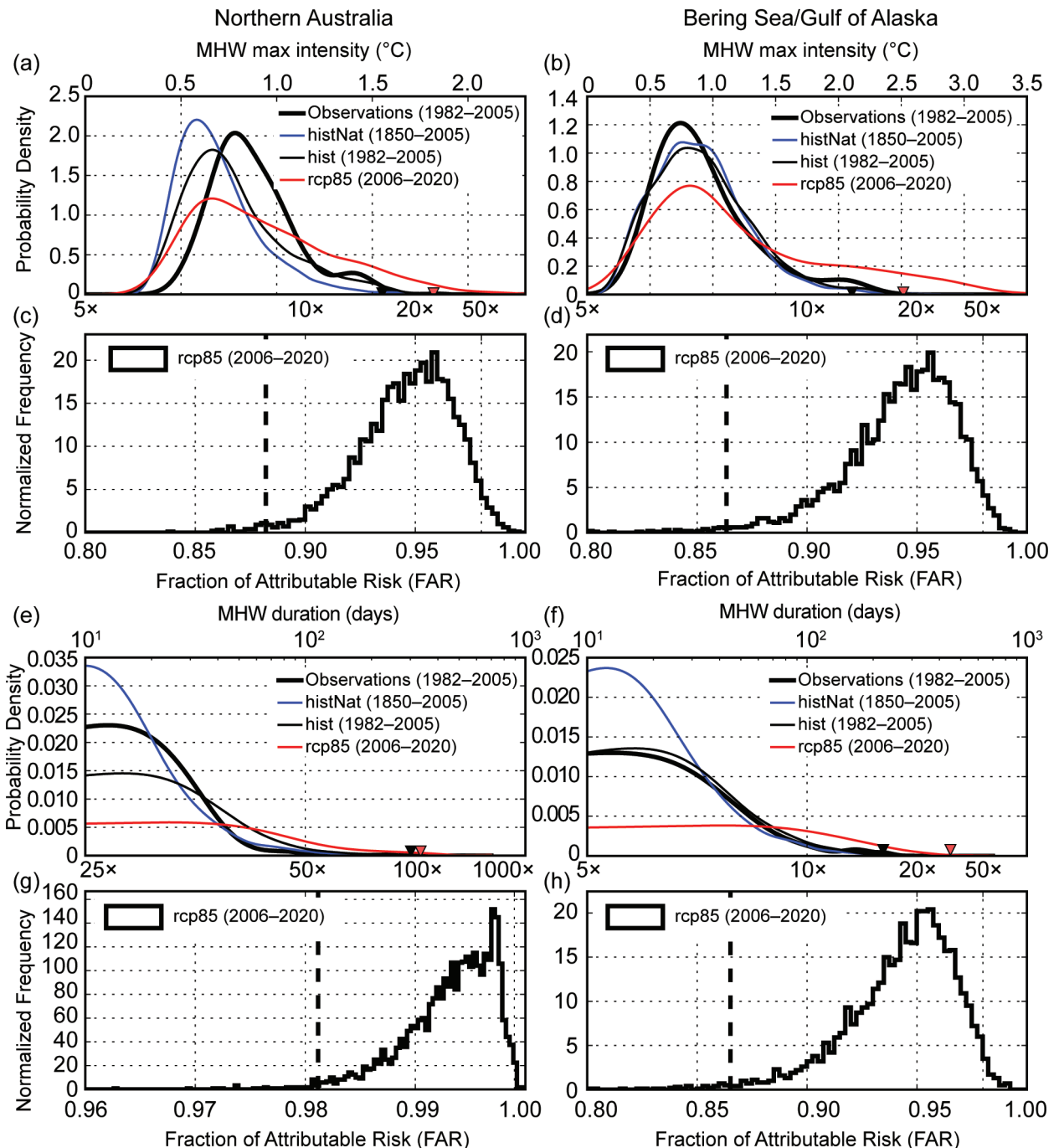
FIG. 9.2. Attribution of the 2016 MHWs in (left) NA and (right) BSGA using global climate models. Probability distributions of (a),(b) maximum intensity, and (e),(f) duration of all MHWs detected from the observations (thick black line) and the ensemble of CMIP5 historical simulations over 1982–2005 (thin black line), historical-Nat simulations (blue line), and RCP8.5 simulations over 2006–20 (red line). Black and red triangles indicate the properties of the event being attributed and of the 2016 event, respectively. The distribution of FAR values from the RCP85 runs for (c),(d) maximum intensity, and (g),(h) duration (distribution of all bootstrapped values: solid line; 1st percentile: dashed line).

REFERENCES

Belles, J., 2016: The blob is back: Anomalous warmth returns to the North Pacific Ocean. ("The Weather Channel" story, with related video.) [Available online at https://weather.com/news/climate/news/the-blob-pacific-ocean-temperatures/.]

Cavole, L. M., and Coauthors, 2016: Biological impacts of the 2013–2015 warm-water anomaly in the Northeast Pacific: Winners, losers, and the future. *Oceanography*, **29** (2), 273–285, doi:10.5670/oceanog.2016.32.

Hobday, A. J., and Coauthors, 2016: A hierarchical approach to defining marine heat waves. *Prog. Oceanogr.,* **141**, 227–238, doi:10.1016/j.pocean.2015.12.014.

Hughes, T. P., and Coauthors, 2017: Global warming and recurrent mass bleaching of corals. *Nature*, **543**, 373–377, doi:10.1038/nature21707.

Kennedy, J. J., N. A. Rayner, R. O. Smith, D. E. Parker, and M. Saunby, 2011a: Reassessing biases and other uncertainties in sea surface temperature observations measured in situ since 1850: 1. Measurement and sampling uncertainties. *J. Geophys. Res.*, **116**, D14103, doi:10.1029/2010JD015218.

——, ——, ——, ——, and ——, 2011b: Reassessing biases and other uncertainties in sea surface temperature observations measured in situ since 1850: 2. Biases and homogenization. *J. Geophys. Res.*, **116**, D14104, doi:10.1029/2010JD015220.

King, A. D., G. J. van Oldenborgh, D. J. Karoly, S. C. Lewis, and H. Cullen, 2015: Attribution of the record high Central England temperature of 2014 to anthropogenic influences. *Environ. Res. Lett.*, **10**, 54002, doi:10.1088/1748-9326/10/5/054002.

Lewis, S. C., and D. J. Karoly, 2013: Anthropogenic contributions to Australia's record summer temperatures of 2013. *Geophys. Res. Lett.*, **40**, 3705–3709, doi:10.1002/grl.50673.

Oliver, E. C. J., 2015: Marine Heat waves detection code (Python module). [Available online at http://github.com/ecjoliver/marineHeat waves.]

Oliver, E. C. J., J. A. Benthuysen, M. L. Bindoff, A. J. Hobday, N. J. Holbrook, C. N. Mundy, and S. E. Perkins-Kirkpatrick, 2017: The unprecedented 2015/16 Tasman Sea marine heatwave. *Nat. Comm.*, **8**, 16101, doi:10.1038/ncomms16101.

Reynolds, R. W., T. M. Smith, C. Liu, D. B. Chelton, K. S. Casey, and M. G. Schlax, 2007: Daily high-resolution-blended analyses for sea surface temperature. *J. Climate*, **20**, 5473–5496, doi:10.1175/2007JCLI1824.1.

Taylor, K. E., R. J. Stouffer, and G. A. Meehl, 2012: An overview of CMIP5 and the experiment design. *Bull. Amer. Meteor. Soc.*, **93**, 485–498, doi:10.1175/BAMS-D-00094.1.